Biosensors and Bioelectronics 171 (2021) 112725

Contents lists available at ScienceDirect

Biosensors and Bioelectronics

journal homepage: http://www.elsevier.com/locate/bios

Processable and nanofibrous polyaniline:polystyrene-sulphonate (nano-PANI:PSS) for the fabrication of catalyst-free ammonium sensors and enzyme-coupled urea biosensors

Sinan Uzunçar [a,b], Lingyin Meng [a], Anthony P.F. Turner [a,c], Wing Cheung Mak [a,*]

[a] Biosensors and Bioelectronics Centre, Division of Sensor and Actuator Systems, Department of Physics, Chemistry and Biology, Linköping University, 581 83, Linköping, Sweden
[b] Environmental Engineering Department, Engineering Faculty, Zonguldak Bülent Ecevit University,67100, Zonguldak, Turkey
[c] SATM, Cranfield University, Bedfordshire, MK430AL, UK

ARTICLE INFO

Keywords:
Nanofibre
Processable PANI:PSS
Doping/de-doping
Ammonium
Urea
Biosensors

ABSTRACT

Tailoring conducting polymers (CPs) such as polyaniline (PANI) to deliver the appropriate morphology, electrochemical properties and processability is essential for the development of effective polymer-based electrochemical sensors and biosensors. Composite PANI electrodes for the detection of ammonium (NH_4^+) have been previously reported, but have been limited by their reliance on the electrocatalytic reaction between NH_4^+ and a metal/nano-catalyst. We report an advanced processable and nanofibrous polyaniline:polystyrene-sulphonate (nano-PANI:PSS) as a functional ink for the fabrication of catalyst-free NH_4^+ sensors and enzyme-coupled urea biosensors. The PSS provides both a soft-template for nanofibre formation and a poly-anionic charge compensator, enabling the detection of NH_4^+ based on an intrinsic doping/de-doping mechanism. The nanostructured morphology, chemical characteristics and electrochemical properties of the nano-PANI:PSS were characterised. We fabricated 3D-hierarchical sensor interfaces composed of inter-connected nano-PANI:PSS fibres (diameter of ~50.3 ± 4.8 nm) for the detection of NH_4^+ with a wide linear range of 0.1–11.5 mM ($R^2 = 0.996$) and high sensitivity of 106 mA M^{-1} cm^{-2}. We further demonstrated the coupling of the enzyme urease with the nano-PANI:PSS to create a urea biosensor with an innovative biocatalytic product-to-dopant relay mechanism for the detection of urea, with a linear range of 0.2–0.9 mM ($R^2 = 0.971$) and high sensitivity of 41 mA M^{-1} cm^{-2}. Moreover, the nano-PANI:PSS-based sensors show good selectivity for the detection of $NH_4^+$and urea in a urine model containing common interfering molecules. This processable and fibrous nano-PANI:PSS provides new advance on CP-based transducer materials in the emerging field of printed organic sensors and biosensors.

1. Introduction

Ammonium (NH_4^+) and urea are the main sources of nitrogen pollutants associated with fertiliser production, oil refining, the fermentative food industry and anaerobic wastewater treatment (Dhamole et al., 2015; Tallaksen et al., 2015). Emerging sensor technologies for the detection of NH_4^+ and urea are important in the fields of environmental science and health, with respect to the nitrogen cycle and nitrogen metabolism (Li et al., 2016; Pundir et al., 2019; Stern and Mozdziak 2019) and metabolism driven by mediated electron transfer of microorganisms (Liu et al., 2018). Electrochemical sensors based on potentiometric ion-selective electrodes for the detection of NH_4^+ (Benco et al., 2003; Guinovart et al., 2013) and urease-coupled NH_4^+ ion-selective electrodes for the detection of urea (Eggenstein et al., 1999; Walcerz et al., 1998) have been widely reported. However, there are several limitations associated with the potentiometric technique, such as the membrane potential being affected by the ionic strength of the solution and potential drift during a sequence of measurements (Cosio et al., 2012). In contrast, voltametric and amperometric NH_4^+ and urea sensors (Yamamoto and Senda 1993), which measure a current response, have the advantages of speed, linearity, higher sensitivity and resistance to the effect of ionic strength.

Conducting polymers (CPs), such as polypyrrole (PPY), poly(3,4-ethylenedioxythiophene) (PEDOT) and polyaniline (PANI), exhibit unique reversible doping/de-doping properties (Zhou and Shi 2016), ionic-electronic conductivity and biocompatibility (He et al., 2019), and

* Corresponding author.
E-mail address: wing.cheung.mak@liu.se (W.C. Mak).

https://doi.org/10.1016/j.bios.2020.112725
Received 18 August 2020; Received in revised form 28 September 2020; Accepted 12 October 2020
Available online 17 October 2020

have therefore attracted considerable attention as advanced electrode materials for amperometric electrochemical sensors and biosensors (Aydemir et al., 2016; Meng et al., 2020a). Among all CPs, PANI has the advantages of ease of synthesis, low cost, high chemical stability and tunable redox properties (Dhand et al., 2011), as well as good anti-fouling properties in paints (Baldissera et al., 2015) and on sensor surfaces (Hui et al., 2017). Moreover, PANI has unique selectivity for the detection of non-charged ammonia (NH_3) via a reversible doping/de-doping mechanism through the interaction between the lone pair electrons on the nitrogen atom of PANI and NH_3 (Tanguy et al., 2018). However, the detection of cationic NH_4^+ with PANI required modification of the polymer with Nafion to provide a terminated sulphonate group as charge compensator during the doping/de-doping process (Cho and Huang 1998). Alternatively, PANI-based catalytic NH_4^+ sensors and enzyme-coupled biosensors prepared by electrochemically polymerised PANI composites such as PANI-copper-Nafion (Zhybak et al. 2016a, 2017), PANI-platinum–carbon (Strehlitz et al., 2000), PANI-platinum-Nafion (Stasyuk et al., 2012) and PANI-gold-Nafion (Luo and Do 2004) have also been reported. For the PANI-copper-Nafion composite, the detection of NH_4^+ is via an indirect pH-driven conversion of NH_4^+ to NH_3, leading to the formation of NH_3/copper complexes, followed by electrochemical detection of the NH_3/copper complex (Zhybak et al. 2016a, 2016b). For the PANI-platinum-Nafion composite, the detection of enzymatically-generated NH_4^+ has similarly been reported to be led by the pH-driven conversion of NH_4^+ to NH_3, followed by electrocatalytic oxidation of NH_3 associated with the oxidation of PANI (Strehlitz et al., 2000), while other research groups suggested that the NH_3 interacts with the platinum to generate a signal response (Jia et al., 2011).

The challenges of effective PANI-based NH_4^+ sensing lay in the chemical nature on the polymer backbone of PANI, which has poor selectivity and diffusion characteristics towards cationic molecules (i.e. NH_4^+) (Hirai et al., 1988), the close-structure of PANI with a limited specific surface area for PANI/NH_4^+ interaction, as well as the poor processability of PANI for scalable sensor fabrication. Recently, several physiochemical strategies have been introduced to improve the performance of CP-based sensors, such as using nanostructured CPs with increased active surface area (Luo et al., 2017; Meng et al., 2020b; Pal et al., 2016; Travas-Sejdic et al., 2014; Vagin et al., 2016; Wannapob et al., 2017) and modulating the surface charge of CPs to facilitate the diffusion of analyte towards sensor surface (Meng et al. 2018, 2019). Moreover, the incorporation of polyelectrolyte such as polystyrene sulphonate (PSS) could improve the stability and processability of CPs such as the use of colloidal PANI:PSS for ink-jet printing (Jang et al., 2007) and as a hole transport material for perovskite solar cells (Lee et al., 2017). Therefore, tailoring the physicochemical properties of PANI by combining nanostructured morphology with improved cationic NH_4^+ selectivity and good processability was the preferred route for the development of a catalyst-free NH_4^+-sensitive PANI for sensing and biosensing applications.

In this work, we developed a processable and nanofibrous PANI:PSS (nano-PANI:PSS) as a functional ink for the fabrication of catalyst-free NH_4^+ sensors. The PSS provides both a soft-template for nanofibre formation and a poly-anionic charge compensator enabling the detection of NH_4^+ by the nano-PANI:PSS based on a doping/de-doping mechanism. The morphology, chemical characteristics and electrochemical properties of the nano-PANI:PSS were characterised. We demonstrated the fabrication of 3D-hierarchical sensor interfaces composed of nano-PANI:PSS_n for the quantitative detection of NH_4^+ which delivered good sensitivity and a wide linear range. We further demonstrated the coupling of the enzyme urease with the nano-PANI:PSS_n to create a urea biosensor exploiting this innovative catalytic product-to-dopant relay mechanism.

2. Experimental

2.1. Materials

Aniline monomer (99.0%), ammonium persulfate (APS, $(NH_4)S_2O_8$, 98.0%), hydrogen chloride solution (HCl, 1M), poly(sodium 4-styrene sulphonate) (PSS, M_w: ~70,000), dipotassium hydrogen phosphate (K_2HPO_4, ≥99%), potassium dihydrogen phosphate monobasic (KH_2PO_4, ≥99.99%), disodium hydrogen phosphate (Na_2HPO_4), ammonium chloride (NH_4Cl), urea ($CO(NH_2)_2$), uric acid, ascorbic acid, creatinine, glucose, glutaraldehyde solution (GA, 50% w/v) and urease with activities of ≥ 600,000 units/g from *Canavalia ensiformis* (Jack bean) were purchased from Sigma-Aldrich (USA). Capillary pore membrane (CPM) discs (RoTrac®, ref-No: 0325,110) were from Oxyphen AG (Wetzikon, Germany). Phosphate buffer solution (PBS, pH 7, 10 mM) was prepared by mixing K_2HPO_4 and NaH_2PO_4 stock solution. Milli-Q water (18.2 MΩ) was utilised to prepare all solutions.

2.2. Synthesis of water-processable and fibrous nano-PANI:PSS dispersion

Processable and fibrous nano-PANI:PSS was prepared via chemical polymerisation of the aniline monomer with PSS and HCl as a template and dopant, respectively. Firstly, a stock aniline solution was mixed with HCl (1 M) at a volume ratio of 1:10 (v/v) and incubated with a programmable rotator (Multi-Bio-RS-24, BioSan) for 4 h at room temperature under dark conditions to obtain anline:HCl with a concentration of 1.28 M aniline. The aniline:HCl mixture was then mixed with PSS solution of various concentrations (13.8, 34.5, and 55.2 mg mL^{-1} in HCl (1M)) at a volume ratio of 1:3 (v/v) with a final concentration of 0.32 M aniline and incubated for 4 h at room temperature under dark conditions. Chemical polymerisation was initiated by mixing the resulting mixture with APS (0.15 mM) at a volume ratio of 1:1 (v/v) and allowing it to react for 24 h with gentle shaking at room temperature in the dark. The resulting nano-PANI:PSS was washed by centrifugation (8251×*g*, 5 min) followed by redispersion in Milli-Q water, and the washing procedure was repeated for three times. Finally, the nano-PANI:PSS was dispersed in 5 mL Milli-Q water and stored in the dark at room temperature for further experiments. The polymer composites synthesised using different PSS concentrations were denoted as PANI:PSS_n and PANI:$PSS_{2.5n}$ and PANI:PSS_{4n}, respectively.

2.3. Fabrication of the GCE/nano-PANI:PSS sensing electrode

Glassy-carbon electrodes (GCE, 3 mm diameter) were polished with 1, 0.3, and 0.5 mm α-alumina slurry successively then washed with deionised water, sonicated in ultra-pure water, and dried under nitrogen. Then, the stock nano-PANI:PSS solution was resuspended by a gentle vortex. 1 μL of the nano-PANI:PSS solution was deposited onto the GCE and allowed to dry for 20 min at room temperature.

2.4. Preparation of GCE/nano-PANI:PSS_n/CPM-urease electrode

A stock urease enzyme solution (10 units/μL) was prepared by dissolving the enzyme powder with 20 mM PBS. An aliquot of urease solution (3 μL) was then deposited onto a CPM disc, allowed to adsorb and then dried at room temperature. The urease CPM disc was crosslinked with GA vapour in a sealed container for 20 min inside a fume hood. The urease CPM was washed with PBS to remove unbound enzyme. Finally, the urease-CPM was assembled onto the surface of the nano-PANI:PSS electrode with a ~1 mm gap with a tailor-designed double-rings membrane holder (Fig. S1).

2.5. Characterisation and electrochemical measurements

Scanning electron microscopy (SEM) images were obtained with a

LEO 155 Gemini (Zeiss, OR, USA). The average diameter of the nano-PANI:PSS fibre was calculated by measuring the diameter of 15 individual fibres from the SEM image and the distribution of the data was presented as the standard deviation of the 15 measurements. Absorption spectra of the nano-PANI:PSS were measured with a Cary 50 UV–vis Spectrometer (Varian Inc., CA, USA). The zeta potential was determined using a Zetasizer Nano ZS90 with 3 repeated measurements (Malvern Instruments Ltd., Worcestershire, UK). FT-IR measurements were carried out using a PE 100 FT-IR spectrometer (PerkinElmer, Waltham, MA, USA).

Electrochemical measurements were performed with an IviumStat. XR electrochemical analyser (Eindhoven, Netherlands). A three-electrode cell with a GCE working electrode (0.07 cm^2 surface area) and a platinum wire auxiliary electrode and an Ag/AgCl (3 M KCl) reference electrode were utilised in the electrochemical measurements. Cyclic voltammetry (CV) was performed between a predetermined potential window at a scan rate of 50 mV s^{-1}. Square wave voltammetry (SWV) measurements were performed according to the following protocol: pretreatment of 60 s at −0.8 V, potential window of 0–0.9 V, pulse amplitude of 50 mV, frequency of 10 Hz, and a potential step of 5 mV. The signal responses of the nano-PANI:PSS_n electrodes and the nano-PANI:PSS_n/CPM-urease bioelectrodes with different concentrations of NH_4^+ and urea were measured with 3 repeated measurements and the distribution of the data (i.e. the error bar) was presented as the standard deviation of the 3 repeated measurements.

3. Results and discussion

3.1. Optimisation and characterisation of processable nanofibrous PANI:PSS

The introduction of poly-anionic PSS rendered the PANI:PSS solution processable as well as serving as a soft-template for nanofibre formation. The effect of PSS content in the polymer composite on electrochemical behaviour with NH_4^+ was investigated by comparing three different composites, nano-PANI:PSS_n, nano-PANI:$PSS_{2.5n}$ and nano-PANI:PSS_{4n} using CV. As shown in Fig. S2, the nano-PANI:PSS_n demonstrated a well-defined oxidation (i.e. de-doping) peak with a high current response at a low potential, which was chosen for further investigation hereafter. The dispersibility and morphology of the synthesised processable fibrous-structured nano-PANI:PSS_n were characterised. Fig. 1a shows the synthesised nano-PANI:PSS is well-dispersed in water without observable sedimentation, indicating the good dispersion stability of the nano-PANI:PSS_n originating from the negatively charged PSS. The dispersibility of the nano-PANI:PSS_n was further qualified by zeta potential analysis. The zeta potential of the nano-PANI:PSS_n was -30.6 ± 10.7 mV (Fig. S3), which is attributed to the negatively-charged sulphonate group of PSS. Moreover, the zeta potential of the nano-PANI:PSS_n with a magnitude of ~30 mV is considered sufficient to maintain a stable colloidal dispersion by electrostatic repulsion force (Lowry et al., 2016). The compacted and fairly uniform film in Fig. 1b was formed by deposition of the processable nano-PANI:PSS_n ink via simple drop-casting method. The film morphology of the corresponding fibrous

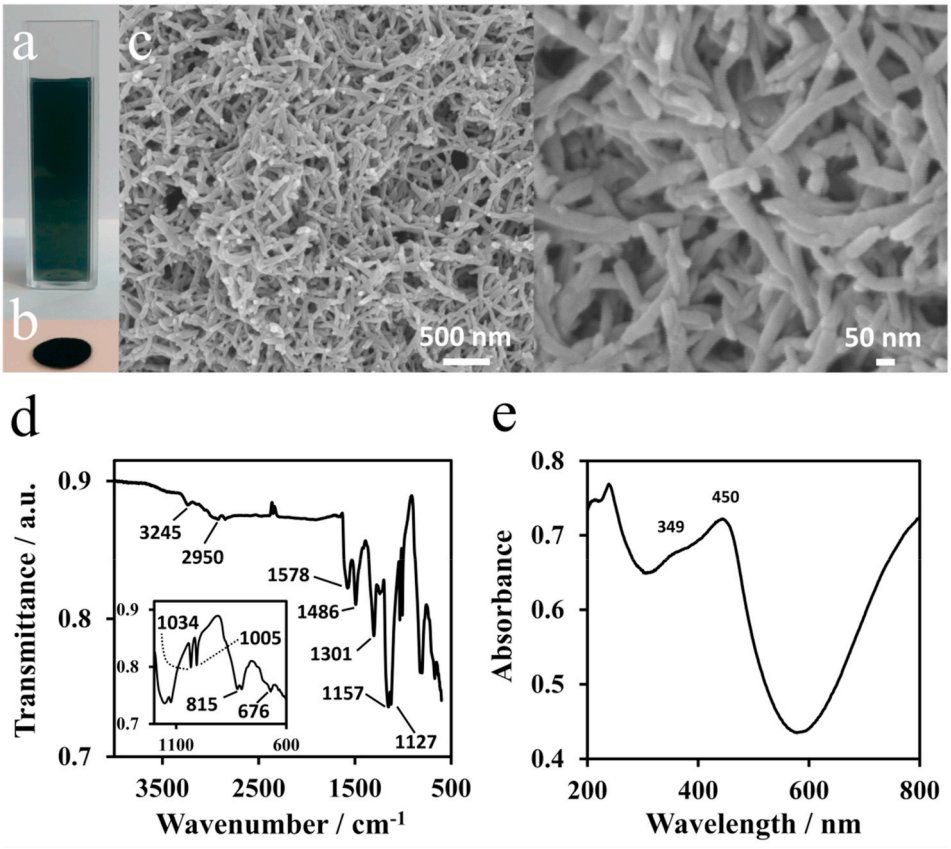

Fig. 1. (a) Digital photograph of the fibrous-structured nano-PANI:PSS_n dispersion in aqueous solution and (b) corresponding deposited nano-PANI:PSS_n film on a glass substrate; (c) SEM images of the fibrous-structured nano-PANI:PSS_n at different scales; (d) FT-IR spectrum and (e) UV–Vis spectrum of the nano-PANI:PSS_n.

nano-PANI:PSS_n film was evaluated via SEM as shown in Fig. 1c. The nano-PANI:PSS_n film is composed of a 3D inter-connected nano-PANI:PSS_n nanofibre network with an estimated fibre diameter of ~50.3 ± 4.8 nm (n = 15, Fig. S3). The developed nano-PANI:PSS_n combines the advantages of good processability and nanofibrous morphology and is therefore useful as functional ink for facile preparation of 3D-hierarchical conducting polymer interfaces with an increased surface area.

The chemical characteristics of the nano-PANI:PSS_n were characterised by FT-IR and UV–vis spectroscopy as shown in Fig. 1d and e, respectively. In the FT-IR spectrum, the bands at 3245 and around 2950 cm^{-1} can be ascribed to the N–H stretching of secondary aromatic amine and aromatic C–H stretching, respectively (Bocchini et al., 2013; Hu et al., 2016; Kim et al., 2002). Two distinctive bands at 1578 and 1486 cm^{-1} corresponding to C═C stretching vibration of quinonoid and benzenoid rings from the oxidised form of PANI can be seen in the spectrum (Bocchini et al., 2013; Cho et al., 2014; Kim et al., 2002; Su 2015). The band at 1301 cm^{-1} belongs to the aromatic C–N stretching vibration of the secondary aromatic amine group (Cho et al., 2014; Kulkarni et al., 2004; Su 2015). Besides that, the bands at 1127, 1005 and 815 cm^{-1} are assigned to the benzene ring in-plane vibration, in-plane bending vibration and out-of-plane bending vibration, respectively (Bocchini et al., 2013; Cho et al., 2014). The symmetric and asymmetric stretching modes of SO_3^{2-} group from the PSS dopant can be found at 1157/1127 and 1034/1005 cm^{-1}, respectively (Bocchini et al., 2013; Cho et al., 2014; Hu et al., 2016). The band at 676 cm^{-1} corresponds to C–S stretching vibration mode of the benzenoid ring and suggests the successful doping of PSS into PANI. The UV–vis spectroscopy shows a typical band at around 359 nm attributed to the π-π* transition of benzenoid ring. The band at 450 nm corresponds to polaron absorption ascribed to the protonated conductive PANI (Bocchini et al., 2013; Luo et al., 2013; Su 2015).

3.2. Electrochemical characteristics of nano-PANI:PSS_n to ammonium

The characteristic redox states of nano-PANI:PSS_n were studied using CV in 0.1 M HCl (Fig. S4). Two distinct sets of redox peaks corresponding to the redox reactions among leucoemeraldine, partially oxidised emeraldine and fully oxidised pernigraniline states indicate the typical electroactivity of PANI, which is consistent with previous reports (Dias et al., 2007; Song and Choi 2013; Wu et al., 2005). The electrochemical behaviour of the nano-PANI:PSS_n electrode towards NH_4^+ was evaluated in 10 mM PBS (pH 7) as shown in Fig. 2. In the absence of NH_4^+, the nano-PANI:PSS_n electrode displayed a pair of redox peaks related to the conversion of leucoemeraldine/emeraldine states at −0.18 and 0.4 V, respectively. After the addition of NH_4^+, both the anodic and cathodic currents increased. The mechanism for the increased response towards NH_4^+ at the nano-PANI:PSS_n interface is described in Eq. (1).

$$[\text{nano-PANI}^+_{(ox)}\text{: PSS}^-] + NH_4^+ + e^- \leftrightarrow [\text{nano-PANI}_{(red)}\text{: PSS}^-\ (NH_4)^+] \quad .1$$

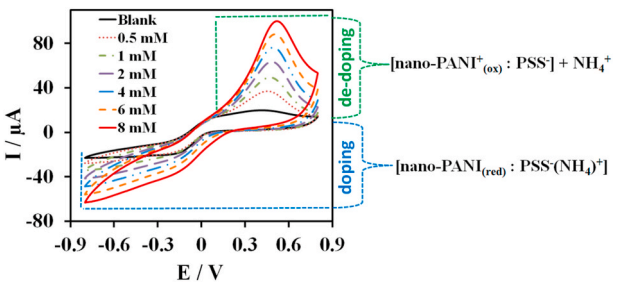

Fig. 2. Sensing mechanism of nano-PANI:PSS_n electrode to NH_4^+ characterised by CV response to different concentration of NH_4^+ (0, 0.5, 1, 2, 4, 6, 8 mM) in 10 mM PBS (pH 7), scan rate of 50 mV s^{-1}.

Initially, the emeraldine state of nano-PANI possesses a positively-charged backbone, and the negatively-charged PSS serves as a non-mobile poly-anionic charge compensator within the polymer matrix (i.e. nano-$PANI^+_{(ox)}$:PSS_n^-). In the negative scan of the CV, the positively-charged PANI backbone in nano-$PANI^+_{(ox)}$:PSS_n^- matrix is reduced to a neutral state without charge (i.e. nano-$PANi_{(red)}$:PSS_n^-), while the positively-charged NH_4^+ molecules insert into the nano-PANI:PSS_n matrix (i.e. nano-$PANI_{(red)}$:PSS^- $(NH_4)^+$). The insertion of NH_4^+ into the nano-PANI:PSS_n matrix during the reduction process is defined as the doping of NH_4^+. In the subsequent positive scan, the reduced state of the nano-$PANI_{(red)}$ is reversibly oxidised back to the nano-$PANI^+_{(ox)}$ with the positively-charged backbone, leading to the release of NH_4^+ from the polymer matrix, which is defined as the de-doping of NH_4^+. It can be seen from Fig. 2 that the de-doping process of NH_4^+ from the nano-PANI:PSS_n resulted in a well-defined oxidation peak, which is favourable for the sensing of NH_4^+ with high sensitivity. Besides that, it can be noted that the anodic and cathodic currents increased gradually as the concentration of NH_4^+ increases for quantitative detection of NH_4^+ with the nano-PANI:PSS_n electrode. By contrast, the doping/de-doping of NH_4^+ in PANI:Cl with mobile small molecular weight anions could not be realised, owing to the absence of non-mobile poly-anionic charge compensator effect (Supporting Fig. S5).

Fig. 3 shows the influence of the operational potential range on the doping/de-doping degree of nano-PANI:PSS_n with NH_4^+, with a constant oxidation potential (OP) of 0.8 V in the positive scan and gradually increased reduction potential (RP) from 0 to −0.8 V in the negative scan. As can be seen from Fig. 3a, in the absence of NH_4^+, the anodic currents between 0 and 0.8 V in positive scan showed only a slight increase with the decrease of RP from 0 to −0.8 V, which might be ascribed to the sluggish increase of doping (at negative potential) and de-doping (at positive potential) of Na^+ or K^+ in the blank PBS (10 mM, pH 7). While, in the presence of 4 mM NH_4^+, the nano-PANI:PSS_n electrode (Fig. 3b) displayed a significantly increased cathodic reduction current and anodic oxidation current compared to those without NH_4^+. When the negative scan range extended from 0 to −0.8 V, the reduction degree of nano-PANI:PSS_n increased, causing a higher doping level of NH_4^+ into the nano-PANI:PSS_n, and thus the corresponding anodic current signal increased with a positively shifted peak potential.

3.3. Nano-PANI:PSS_n interface for detection of ammonium and urea

A 3D-hierarchical sensor interface composed of assembled nano-PANI:PSS_n was fabricated for quantitative detection of NH_4^+ as shown in Fig. 4a. Owing to the well-defined de-doping (oxidation) peak in the positive scan range of the nano-PANI:PSS_n towards NH_4^+, SWV was performed over the range of 0–0.9 V in 10 mM PBS (pH 7) for the detection of the NH_4^+ concentration based on the de-doping level. Fig. 4b

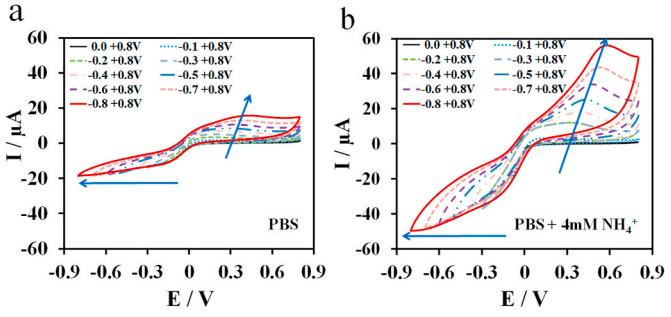

Fig. 3. The effect of potential range on doping/de-doping degree of the nano-PANI:PSS_n in (a) 10 mM PBS and (b) 10 mM PBS containing 4 mM NH_4^+, scan rate of 50 mV s^{-1}.

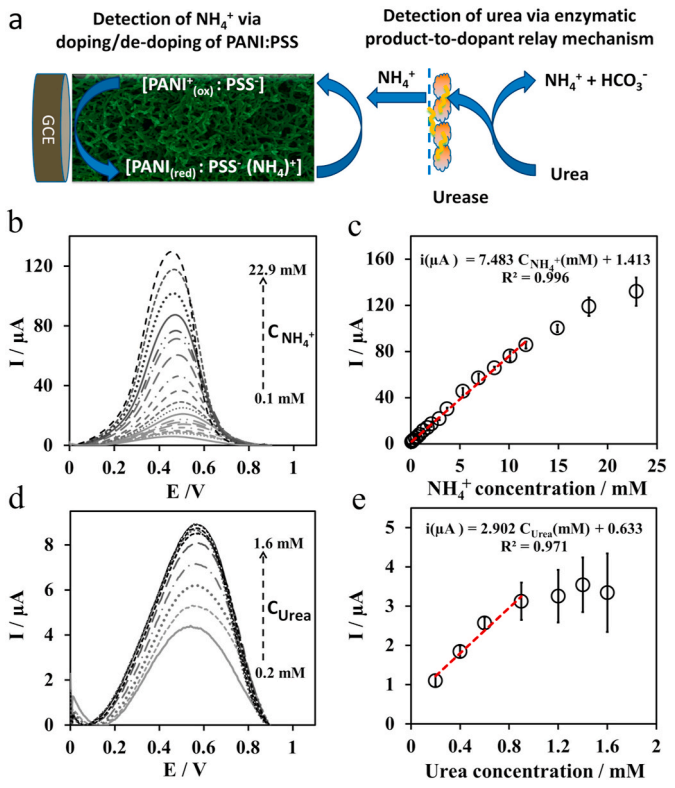

Fig. 4. (a) Schematic illustrating the NH_4^+ sensing mechanism of the nano-PANI:PSS_n sensor and the coupling of the enzyme urease with nano-PANI:PSS_n as a urea biosensor with an innovative catalytic product-to-dopant relay mechanism; (b) the SWV responses of nano-PANI:PSS_n sensor towards successive addition of NH_4^+ in 10 mM PBS (pH 7); (c) corresponding calibration curve for NH_4^+ sensing, n = 3; (d) SWV response of nano-PANI:PSS_n/CPM-urease biosensor towards successive addition of urea in 10 mM PBS (pH 7); (e) corresponding calibration curve for urea biosensing, n = 3.

displays the SWV response curves for the blank (solid black curve) and the successive additions of NH_4^+ up to 22.9 mM. An increase in the NH_4^+ concentration resulted in well-defined de-doping peaks with an increasing trend in the peak currents. The corresponding calibration curve in Fig. 4c shows the responses of peak current signals were linearly proportional to the NH_4^+ concentration over a wide range of 0.1–11.7 mM with a linear regression of i (µA) = 7.843 $C_{NH_4^+}$ (mM) + 1.413 (R^2 = 0.996) and sensitivity of 106 ± 1.8 mA M^{-1} cm^{-2}. The limit of detection (LOD) value was calculated to be 26.9 µM (3σ/*s*, where σ is the standard deviation of the 10 blanks, *s* is the slope of the calibration curve). The analytical performance of the catalyst-free nano-PANI:PSS_n NH_4^+ sensor was compared with previously reported PANI-metal composite-based NH_4^+ sensors, such as CuO_2/Nafion/PANI (Zhybak et al., 2016b), platinum-carbon/PANI (Strehlitz et al., 2000), platinum/Nafion/PANI (Stasyuk et al., 2012), Au/Nafion/PANI (Luo and Do 2004) and Al_2O_3–Au/Nafion/PANI (Do et al., 2018) to illustrate the wider linear range and a good sensitivity resulting from the high surface area of the fibrous structure of the nano-PANI:PSS_n (Table S1). Moreover, it is important to note that our nano-PANI:PSS_n is processable, which thus facilitates simple and scalable preparation of the PANI-based NH_4^+ sensors via deposition of the nano-PANI:PSS_n solution, while the previously reported PANI-metal composite based NH_4^+ sensors were prepared by electrochemical polymerisation cycles.

We further demonstrated the coupling of urease with the NH_4^+ sensitive nano-PANI:PSS_n as a urea biosensor with an innovative catalytic product-to-dopant relay mechanism, in which the urea is enzymatically-catalysed by urease generating the NH_4^+ product, followed by the diffusion of NH_4^+ into nano-PANI:PSS_n fibrous network triggering the doping/de-doping reaction at PANI:PSS_n interface (Fig. 4a). The response of the nano-PANI:PSS_n/CPM-urease biosensor towards urea was evaluated by SWV in 10 mM PBS (pH 7). As shown in Fig. 4d, the oxidation peak currents increased with successive additions of urea up to 1.6 mM. The calibration curve of the peak current as a function of the urea concentration in Fig. 4e shows a linearly increasing trend over the range 0.2–0.9 mM with a linear regression of i(µA) = 2.901 C_{Urea} (mM) + 0.633 (R^2 = 0.971). The sensitivity of the nano-PANI:PSS_n/CPM-urease biosensor was 41 ± 5.0 mA M^{-1} cm^{-2}, which is higher than previously reported PANI-urease-based urea sensors containing a metal/nano-catalyst (i.e. PANI-metal/nanocomposite), such as Au-ceramic olate/Nafion-PANI/urease (4.2 mA M^{-1} cm^{-2}) (Luo and Do 2004), Pt–C/PANI/PCS-urease (40 mA M^{-1} cm^{-2}) (Strehlitz et al., 2000), Au/PANI-PSS/hydrogel-urease (1.177 mA M^{-1} cm^{-2}) (Sioniewska and Palys 2014), Pt nanoflower/PANI/urease (0.115 mA M^{-1} cm^{-2}) (Jia et al., 2011) and CNT/PANI-GDN/urease (22.9 mA M^{-1} cm^{-2}) (Kumar et al., 2017) (Table S2). The LOD was calculated to be 51.8 µM (3σ/*s*, where σ is the standard deviation of the 10 blanks, *s* is the slope of the calibration curve).

The selectivity of the nano-PANI:PSS_n and the nano-PANI:PSS_n/CPM-urease sensors was studied for the detection of NH_4^+ and urea in a normal urine model (50 times dilution) containing 200 µM of NH_4^+, 20 µM of creatine, 1 µM of ascorbic acid, 3 µM of uric acid, 1 µM of glucose and 200 µM of urea (Tran et al., 2017). Fig. 5a shows the nano-PANI:PSS_n sensor had a relatively high signal response towards NH_4^+, while the signal responses from other interfering molecules were similar to the blank. When the signal response obtained by the nano-PANI:PSS_n electrode for NH_4^+ was normalised to 100%, the signal responses from urea, creatine, ascorbic acid, uric acid, and glucose were only 0.1%, 8.5%, 9.7%, 7.3% and 0.2%, respectively (Fig. 5b). It is important to note that the nano-PANI:PSS_n sensor shows a very low background response (0.1%) towards urea, while after coupling the nano-PANI:PSS_n electrode with urease, the urea response of the nano-PANI:PSS_n/CPM-urease sensor is significantly increased to 42.6%. These results demonstrate that the fibrous nano-PANI:PSS_n interfaces can be used for the selective detection of NH_4^+, and with the subsequent integration of the urease, for urea biosensing.

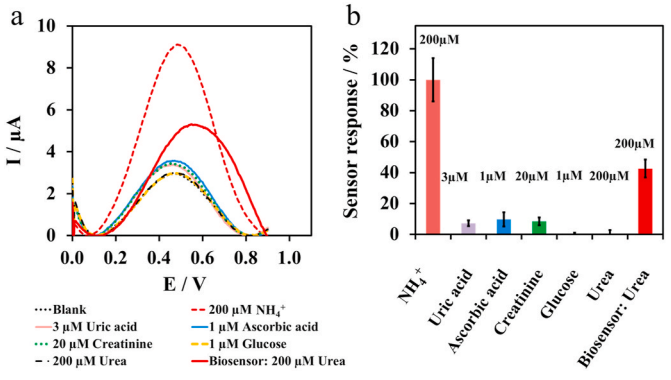

Fig. 5. (a) Selectivity study of GCE/PANI:PSS_n electrode with respect to normal interfering species in urine; (b) Standardised current response for different interfering species.

4. Conclusions

We have demonstrated the development of a novel nano-PANI:PSS combining nanostructured morphology with good processability and cationic NH_4^+ selectivity for the development of catalyst-free nano-PANI:PSS-based NH_4^+ sensors and enzyme-coupled urea biosensors. We explored the unique intrinsic doping/de-doping mechanism of the nano-PANI:PSS for the catalyst-free detection of NH_4^+ without dependence on traditional metal/nano-catalysts. The good processability of nano-PANI:PSS facilitates the scalable fabrication of hierarchical sensor interfaces composed of assembled nano-PANI:PSS fibres via a simple drop-casting method. We also demonstrated the coupling of urease with the nano-PANI:PSS for the fabrication of urea biosensor with an innovative catalytic product-to-dopant relay mechanism. Moreover, the nano-PANI:PSS-based NH_4^+ sensors and enzyme-coupled urea biosensors show good selectivity for the detection of $NH_4^+$and urea in a urine model containing common interfering molecules. Such NH_4^+ sensitive nano-PANI:PSS interface could be used for the fabrication of different biosensor systems by the coupling of different specific enzymes such as arginase and creatinase for the detection of L-arginine and creatinine, respectively.

CRediT authorship contribution statement

Sinan Uzunçar: Formal analysis, Writing - original draft. **Lingyin Meng:** Formal analysis, Writing - review & editing. **Anthony P.F. Turner:** Formal analysis, Writing - review & editing. **Wing Cheung Mak:** Conceptualization, Formal analysis, Writing - review & editing, Supervision.

Declaration of competing interest

We have no conflict of interest to declare.

Acknowledgements

Sinan Uzunçar thanks TUBITAK for financial support through the 2214A-International Research Fellowship Programme.

Appendix A. Supplementary data

Supplementary data to this article can be found online at https://doi.org/10.1016/j.bios.2020.112725.

References

Aydemir, N., Malmstrom, J., Travas-Sejdic, J., 2016. Phys. Chem. Chem. Phys. 18 (12), 8264–8277.
Baldissera, A.F., de Miranda, K.L., Bressy, C., Martin, C., Margaillan, A., Ferreira, C.A., 2015. Mater. Res. 18 (6), 1129–1139.
Benco, J.S., Nienaber, H.A., McGimpsey, W.G., 2003. Anal. Chem. 75 (1), 152–156.
Bocchini, S., Chiolerio, A., Porro, S., Accardo, D., Garino, N., Bejtka, K., Perrone, D., Pirri, C., 2013. J. Mater. Chem. C 1 (33), 5101–5109.
Cho, S., Lee, J.S., Jun, J., Kim, S.G., Jang, J., 2014. Nanoscale 6 (24), 15181–15195.
Cho, W.J., Huang, H.J., 1998. Anal. Chem. 70 (18), 3946–3951.
Cosio, M.S., Scampicchio, M., Benedetti, S., 2012. Chapter 8 - electronic noses and tongues. In: Picó, Y. (Ed.), Chemical Analysis of Food: Techniques and Applications. Academic Press, Boston, pp. 219–247.
Dhamole, P.B., Nair, R.R., D'Souza, S.F., Pandit, A.B., Lele, S.S., 2015. Appl. Biochem. Biotechnol. 175 (2), 748–756.
Dhand, C., Das, M., Datta, M., Malhotra, B.D., 2011. Biosens. Bioelectron. 26 (6), 2811–2821.
Dias, H.V.R., Rajapakse, R.M.G., Krishantha, D.M.M., Fianchini, M., Wang, X.Y., Elsenbaumer, R.L., 2007. J. Mater. Chem. 17 (18), 1762–1768.
Do, J.S., Chang, Y.H., Tsai, M.L., 2018. Mater. Chem. Phys. 219, 1–12.
Eggenstein, C., Borchardt, M., Diekmann, C., Grundig, B., Dumschat, C., Cammann, K., Knoll, M., Spener, F., 1999. Biosens. Bioelectron. 14 (1), 33–41.
Guinovart, T., Bandodkar, A.J., Windmiller, J.R., Andrade, F.J., Wang, J., 2013. Analyst 138 (22), 7031–7038.
He, H., Zhang, L., Guan, X., Cheng, H.L., Liu, X.X., Yu, S.Z., Wei, J., Ouyang, J.Y., 2019. ACS Appl. Mater. Interfaces 11 (29), 26185–26193.
Hirai, T., Kuwabata, S., Yoneyama, H., 1988. J. Electrochem. Soc. 135 (5), 1132–1137.
Hu, C.-W., Kawamoto, T., Tanaka, H., Takahashi, A., Lee, K.-M., Kao, S.-Y., Liao, Y.-C., Ho, K.-C., 2016. J. Mater. Chem. C 4 (43), 10293–10300.
Hui, N., Sun, X.T., Niu, S.Y., Luo, X.L., 2017. ACS Appl. Mater. Interfaces 9 (3), 2914–2923.
Jang, J., Ha, J., Cho, J., 2007. Adv. Mater. 19 (13), 1772–1775.
Jia, W.Z., Su, L., Lei, Y., 2011. Biosens. Bioelectron. 30 (1), 158–164.
Kim, B., Oh, S., Han, M., Im, S., 2002. Polymer 43 (1), 111–116.
Kulkarni, M.V., Viswanath, A.K., Marimuthu, R., Seth, T., 2004. Polym. Eng. Sci. 44 (9), 1676–1681.
Kumar, V., Mahajan, R., Kaur, I., Kim, K.H., 2017. ACS Appl. Mater. Interfaces 9 (20), 16813–16824.
Lee, K., Cho, K.H., Ryu, J., Yun, J., Yu, H., Lee, J., Na, W., Jang, J., 2017. Electrochim. Acta 224, 600–607.
Li, L., Long, Y., Gao, J.M., Song, K., Yang, G.Q., 2016. Nanoscale 8 (8), 4458–4462.
Liu, X.B., Shi, L., Gu, J.D., 2018. Biotechnol. Adv. 36 (7), 1815–1827.
Lowry, G.V., Hill, R.J., Harper, S., Rawle, A.F., Hendren, C.O., Klaessig, F., Nobbmann, U., Sayre, P., Rumble, J., 2016. Environ. Sci. J. Integr. Environ. Res.: Nano 3 (5), 953–965.
Luo, J., Chen, Y., Ma, Q., Liu, R., Liu, X., 2013. RSC Adv. 3 (39), 17866–17873.
Luo, J., Huang, J., Wu, Y.N., Sun, J., Wei, W., Liu, X.Y., 2017. Biosens. Bioelectron. 94, 39–46.
Luo, Y.C., Do, J.S., 2004. Biosens. Bioelectron. 20 (1), 15–23.
Meng, L., Turner, A.P.F., Mak, W.C., 2018. Biosens. Bioelectron. 120, 115–121.
Meng, L., Turner, A.P.F., Mak, W.C., 2019. ACS Appl. Mater. Interfaces 11 (37), 34497–34506.
Meng, L., Turner, A.P.F., Mak, W.C., 2020a. Biotechnol. Adv. 39, 107398.
Meng, L., Turner, A.P.F., Mak, W.C., 2020b. Biosens. Bioelectron. 159, 112181.
Pal, R.K., Farghaly, A.A., Wang, C.Z., Collinson, M.M., Kundu, S.C., Yadavalli, V.K., 2016. Biosens. Bioelectron. 81, 294–302.
Pundir, C.S., Jakhar, S., Narwal, V., 2019. Biosens. Bioelectron. 123, 36–50.
Sioniewska, A., Palys, B., 2014. Electrochim. Acta 126, 90–97.
Song, E., Choi, J.W., 2013. Nanomaterials-Basel 3 (3), 498–523.
Stasyuk, N., Smutok, O., Gayda, G., Vus, B., Koval'chuk, Y., Gonchar, M., 2012. Biosens. Bioelectron. 37 (1), 46–52.
Stern, R.A., Mozdziak, P.E., 2019. J. Anim. Physiol. Anim. Nutr. 103 (3), 774–785.
Strehlitz, B., Grundig, B., Kopinke, H., 2000. Anal. Chim. Acta 403 (1–2), 11–23.
Su, N., 2015. Polymers 7 (9), 1599–1616.
Tallaksen, J., Bauer, F., Hulteberg, C., Reese, M., Ahlgren, S., 2015. J. Clean. Prod. 107, 626–635.
Tanguy, N.R., Thompson, M., Yan, N., 2018. Sensor. Actuator. B Chem. 257, 1044–1064.
Tran, T.Q.N., Das, G., Yoon, H.H., 2017. Sensor. Actuator. B Chem. 243, 78–83.
Travas-Sejdic, J., Aydemir, N., Kannan, B., Williams, D.E., Malmstrom, J., 2014. J. Mater. Chem. B 2 (29), 4593–4609.
Vagin, M.Y., Jeerapan, I., Wannapob, R., Thavarungkul, P., Kanatharana, P., Anwar, N., McCormac, T., Eriksson, M., Turner, A.P.F., Jager, E.W.H., Mak, W.C., 2016. Electrochim. Acta 190, 495–503.
Walcerz, I., Glab, S., Koncki, R., 1998. Anal. Chim. Acta 369 (1–2), 129–137.
Wannapob, R., Vagin, M.Y., Liu, Y., Thavarungkul, P., Kanatharana, P., Turner, A.P.F., Mak, W.C., 2017. ACS Appl. Mater. Interfaces 9 (38), 33368–33376.
Wu, M.Q., Snook, G.A., Gupta, V., Shaffer, M., Fray, D.J., Chen, G.Z., 2005. J. Mater. Chem. 15 (23), 2297–2303.
Yamamoto, Y., Senda, M., 1993. Sensor. Actuator. B Chem. 13 (1–3), 57–60.
Zhou, Q.Q., Shi, G.Q., 2016. J. Am. Chem. Soc. 138 (9), 2868–2876.
Zhybak, M., Beni, V., Vagin, M.Y., Dempsey, E., Turner, A.P.F., Korpan, Y., 2016a. Biosens. Bioelectron. 77, 505–511.
Zhybak, M.T., Fayura, L.Y., Boretsky, Y.R., Gonchar, M.V., Sibirny, A.A., Dempsey, E., Turner, A.P.F., Korpan, Y.I., 2017. Microchim. Acta. 184 (8), 2679–2686.
Zhybak, M.T., Vagin, M.Y., Beni, V., Liu, X.J., Dempsey, E., Turner, A.P.F., Korpan, Y.I., 2016b. Microchim. Acta. 183 (6), 1981–1987.